Bol. Soc. Paran. Mat.
©SPM – E-ISSN-2175-1188
SPM: www.spm.uem.br/bspm

(3s.) **v. 2026 (44) 17** : 1–19.
ISSN-0037-8712
doi:10.5269/bspm.82382

Cross Diffusion Effects on an Unsteady Casson-Nanofluid Flow Past an Inclined Stretching Surface With Magnetic Field and Variable Thermal Conductivity

L. Vishnu Priya, R. Srinivasa Raju, S. Jana Reddy and M. Anil Kumar

ABSTRACT: We aim to solve numerically the problem of non-Newtonian Casson nanofluid flow across a tilted and stretching sheet in two dimensions with electrical conductivity. An ever-changing heat conductivity, cross-diffusion, and a magnetic field will all be considered in the study. These dynamics are governed by the nanofluidic model and the Navier-Stokes equations. A common differential equation can be obtained by applying the appropriate similarity transformations to these equations. To identify numerical answers to the ODEs, the MATLAB 'bvp4c' solver was called upon. Variations in temperature, concentration, and velocity as a function of many physical properties are illustrated graphically. You can see the effects of these flow factors on dimensionless values like the skin-friction coefficient, the heat transfer coefficient (Nusselt number), and the mass transfer coefficient (Sherwood number) in the tables that follow. This conclusion is supported by prior research.

Keywords: Cross diffusion effects, unsteady, variable thermal conductivity, magnetic field, casson fluid, nanofluid, inclined stretching sheet, numerical solutions.

Contents

1. Introduction

Variable thermal conductivity in nanofluids means that the fluid's ability to transfer heat changes depending on things like temperature, nanoparticle concentration, and the properties of the particles. Engineers can design systems that meet specific heat management needs since they can control thermal conductivity by changing the concentration of nanoparticles or the temperature. This change is important because it makes it possible to change the parameters to make heat transfer more efficient. This is a big part of why nanofluids work better in applications like cooling systems for electronics and vehicles, solar water heating systems, industrial processes like grinding and machining, and enhanced oil recovery in the oil and gas industry. To evaluate the effects of varying the thermal conductivity in ternary hybrid nanofluids, Jan et al. [1] subjected a stretched sheet to turbulent boundary conditions along with a magnetic field. A study conducted by Jan et al. examined the effects of various thermal conductivities on the long-distance flow of trihybrid nanofluid. [2]. Researchers Alharbi et al. [3] looked at the flow of Casson nanofluid between two spherical bodies that were thermally and fluidically distinct from one another. The third. Maxwell nanofluids in a uniform magnetic field with a changeable thermal conductivity were studied by Srilatha and colleagues to determine the effect of the solid-fluid interface layer and nanoparticle diameter. The movement of a hybrid nanofluid across a sheet in mixed convective stagnation point flow was investigated by Mahmood et al. [4] under changing slip circumstances and thermal conductivity. [5] The study by Abbasi et al. [6] investigated the flow of a hybrid nanofluid

2020 *Mathematics Subject Classification:* 76W05, 80A20.
Submitted March 04, 2026. Published June 19, 2026.

via a curved conduit whose walls are radius-dependent. How the heat conductivity and curvature variables impact the movement was their primary emphasis. Differences in thermal conductivity and uneven heating were the subjects of Khan et al.'s study. [7]. When studying three-dimensional viscoelastic nanofluid flow induced by a rapidly expanding surface, Alqarni et al. [8] examined the significance of bioconvection. They employed a combination of nonlinear radiative heat transfer and changeable thermal conductivity. Hussain et al. [9] performed a computer analysis of three-dimensional, time-dependent Sutterby nanofluid flow, including variations in thermal conductivity and the dynamics of heat sink-source interactions. Abbas and associates [10] examined unstable micropolar nanofluid flow across a variable Riga stretchable surface characterized by fluctuating thermal conductivity. Fatima and colleagues [11] investigated the three-dimensional analysis of motile microorganisms and heat transmission in viscoelastic nanofluids including nth order chemical processes under circumstances of variable thermal conductivity. Rafique et al. [12] computationally investigated the heat conductivity and viscosity of a magnetohydrodynamic hybrid nanofluid flowing down a sloping cylinder. Mandal [13] investigated the entropy analysis of magneto-convective and chemically reactive nanofluid flow along a stretched cylinder, taking into account variations in thermal conductivity and diffusivity. Bafakeeh and associates. [14] investigated the bio-convective characteristics of viscoelastic micropolar nanofluid, emphasizing variations in thermal conductivity and thermo-diffusion properties. Flow characteristics of Carreau-Yasuda nanofluids were investigated by Akbar and colleagues [15]. Concepts including quadratic convection, fluctuating thermal conductivity, and heat transfer were examined. Researchers Abbas et al. [16] used numerical models to examine the magneto-thermal Marangoni convection flow in a powdery Sutterby hybrid nanofluid whose thermal conductivity can be adjusted. A bioconvection Oldroyd-B nanofluid with controllable thermal conductivity and Arrhenius activation energy was investigated by Ramasekhar and colleagues. The effect of a stretched surface on the fluid was studied. In their study, Aljaloud et al. [18] examined the two-phase stress nanofluid flow caused by a stretching surface, considering the impact of varying temperature conductivity and a magnetic field. The process of magnetohydrodynamic Williamson nanofluid flow over a curved surface, which expands exponentially with changing temperature conductivity, was examined by Ahmed and colleagues [19]. Gangadhar et al. [20] examined multiple convective processes in a Williamson nanofluid flow to determine various ways in which thermal conductivity can modulate. Among the variables that Lawal and colleagues [21] considered were the Eyring-Powell nanofluid flow model's thermal conductivity, viscosity, and the variable nonlinear thermal radiation. Using biomedical models of hybrid nanofluid flow in a balloon-catheterized stenotic artery, Dolui et al. [22] investigated the effects of varying thermal conductivity and an angled magnetic field. Pal and colleagues [23] investigated the behavior of a carbon nanotube-based nanofluid that undergoes magnetohydrodynamic thermoradiative heat transfer as it moves through a porous media with a convective expanding sheet and a changing thermal conductivity. Amjad et al. [24] conducted a study of the Williamson nanofluid double diffusion heat flow model over an exponentially stretching surface with variable thermal conductivity. How entropy is generated in the magnetohydrodynamic peristaltic flow of a Carreau-Yasuda nanofluid along a curved channel was studied by Iqbal and Abbasi [25]. They factored in the Joule heating and altering thermal conductivity. The effect of thermal conductivity and Stefan blowing on the magnetohydrodynamic flow of a Sutterby nanofluid in a porous medium was investigated by Rauf et al. [26]. Research on radiative Williamson hybrid nanofluid flow with varying thermal conductivity was conducted computationally by Zubair and colleagues [27]. While considering the temperature dependence of viscosity and thermal conductivity, Darvesh et al. [28] investigated the flow characteristics of a mixed convective inclined magnetic cross nanofluid. After reviewing the aforementioned sources, the authors came to the realization that no one has ever investigated the unsteady magnetohydrodynamic flow of Casson nanofluid's with variable fluid properties, namely thermal conductivity and diffusion coefficient, in response to temperature changes across an inclined and permeable stretching sheet. This study also takes into consideration mass transfer, cross-diffusion effects, and heat transfer. The cooling procedure, which aims to improve the mechanical characteristics of heated sheets, is significantly affected by the problem. Conventional cooling techniques involving base fluids are inapplicable to these sheets. In order to convert the model equations into ODE's, this study will employ similarity transformation. To obtain numerical values for the model, we employed MATLAB's "bvp4c" approach. Using magnetic nanofluids as coolants in external magnetic fields, this study will examine the effects of non-dimensional regulating parameters on dimensionless

velocity, temperature, concentration profiles, skin friction, Nusselt and Sherwood numbers, and more.

2. Flow Governing Equations

This study investigates the impacts of thermal diffusion and dispersion thermo on an unsteady, incompressible, electrically directing, viscous, two-dimensional, non-Newtonian laminar magneto hydrodynamic boundary layer flow of Casson-Nanofluid directed towards an inclined stretching sheet, accounting for variable thermal conductivity, heat transfer, and mass transfer, via numerical solutions. The authors depicted the problem with a figure, Fig. 1, for this research. The following assumptions are postulated for this work:

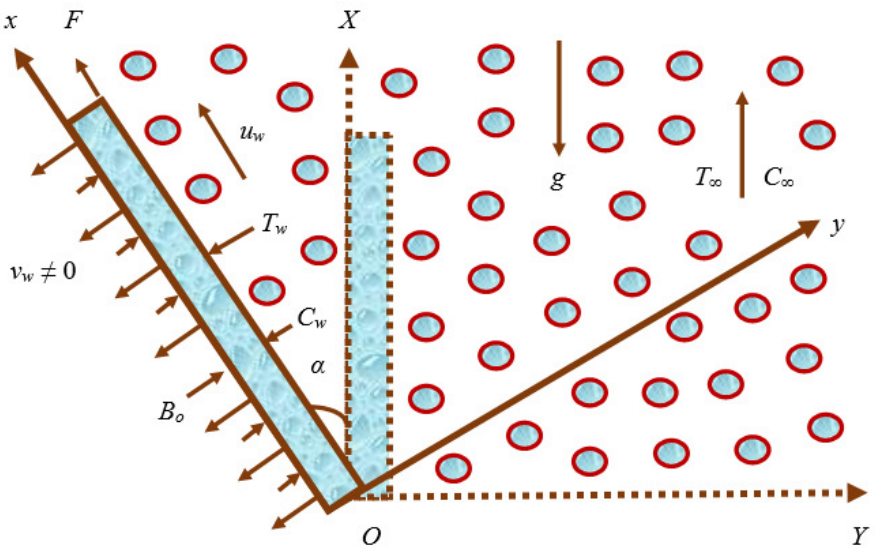

Figure 1: An inclinational Casson-Nanofluid flow diagram.

(i) Variations in temperature and concentration modify the body force term because they change the density. This means that variations in temperature and concentration may create buoyant force.

(ii) Just at right angles to the surface of the stretched sheet is applied a constant magnetic field.

(iii) While the $x-$axis is upright to the expanding exterior and points in the same way as the motion, the $y-$axis is vertical to it.

(iv) The stretching sheet heats the nanofluid and keeps the concentration of chemical species at a steady level.

(v) It is also believed that this flow does not take into account a uniform first-order chemical reaction or heat radiation.

(vi) The inclusion of Fick's and Fourier's laws in the discussion is based on the well-known fact that their descriptions of occurrences are substantially more robust than those associated with the Dufour and Soret effects.

(vii) Theoretically, the temperature of a fluid has a direct correlation with its thermal conductivity and molecular scattering.

(viii) In this case, $v_w(t)$ represents the mass transfer velocity, which is orthogonal to the stretching sheet. $u_w(x,t)$ is the velocity of the stretching sheet, which follows the $x-$axis path of the applied energy F.

(ix) Another common assumption is that $C_w(x,t)$, represents the concentration and $T_w(x,t)$ represents the surface temperature. Away from the stretching sheet, the concentration is C_∞ and the surrounding temperature is T_∞.

(x) Below is the rheological equation that describes a non-Newtonian fluid:

$$\tau = \tau_\infty + \mu\alpha^* \ldots \tag{2.1}$$

The following is an illustration of how to increase the viscosity of Casson fluid using Equation (1):

$$\tau_{ij} = \begin{cases} 2\left(\mu_B + \dfrac{p_y}{\sqrt{2\pi}}\right) e_{ij}, & \pi > \pi_c, \\ 2\left(\mu_B + \dfrac{p_y}{\sqrt{2\pi_c}}\right) e_{ij}, & \pi < \pi_c. \end{cases} \tag{2.2}$$

Where $\pi = e_{ij}e_{ji}$ with e_{ij} represents the $(i,j)^{th}$ component of the Casson fluid's distortion rate and $p_y = \frac{\mu_B\sqrt{2\pi}}{\gamma}$ stands for the yield stress of the fluid.

Based on these concepts and Boussinesq's boundary layer approximations, the flow-controlling model equations are expressed as

The Continuity Formula:

$$\frac{\partial u}{\partial x} + \frac{\partial v}{\partial y} = 0. \tag{2.3}$$

A Formula for Momentum:

$$\left(\frac{\partial u}{\partial t} + u\frac{\partial u}{\partial x} + v\frac{\partial u}{\partial y}\right) = \nu\left(1 + \frac{1}{\gamma}\right)\frac{\partial^2 u}{\partial y^2} - \frac{\sigma B_0^2}{\rho}u + g\beta_T(T - T_\infty)\cos\alpha + g\beta_C(C - C_\infty)\cos\alpha. \tag{2.4}$$

Thermodynamic equation:

$$\frac{\partial T}{\partial t} + u\frac{\partial T}{\partial x} + v\frac{\partial T}{\partial y} = \frac{1}{\rho C_p}\frac{\partial}{\partial y}\left(K(T)\frac{\partial T}{\partial y}\right) + \tau_1\left\{D_B\left(\frac{\partial T}{\partial y}\right)\left(\frac{\partial C}{\partial y}\right) + \frac{D_T}{T_\infty}\left(\frac{\partial T}{\partial y}\right)^2\right\} + \frac{D_m K_T}{C_s}\left(\frac{\partial^2 C}{\partial y^2}\right). \tag{2.5}$$

Equation for the volume concentration of a species' nanoparticles:

$$\frac{\partial C}{\partial t} + u\frac{\partial C}{\partial x} + v\frac{\partial C}{\partial y} = \frac{\partial}{\partial y}\left(D(T)\frac{\partial C}{\partial y}\right) + \frac{D_T}{T_\infty}\left(\frac{\partial T}{\partial y}\right)^2 + \frac{D_M K_T}{T_m}\left(\frac{\partial^2 T}{\partial y^2}\right) \tag{2.6}$$

The relevant boundary conditions for this flow are

$$\begin{aligned} &u = u_w(x,t) = \frac{cx}{1-\delta t}, \qquad v = v_w(t), \qquad T = T_w(x,t), \qquad C = C_w(x,t) \quad \text{at } y = 0, \\ &u \to 0, \qquad T \to T_\infty, \qquad C \to C_\infty \quad \text{as } y \to \infty. \end{aligned} \tag{2.7}$$

Velocity of fluid suction, commonly known as wall mass transfer, follows $v_w = -v_0\sqrt{\frac{\nu c}{1-\delta t}}$. The mass transfer measure across a wall is defined by a constant, v_0 . v_0 is considered suction when it's more than zero, impermeability of the wall when it's equal to zero, and injection when it's smaller than zero. certain a certain amount of time (t) and location (x), the fluid's top-of-the-sheet temperature $T_w(x,t)$ and $C_w(x,t)$ content are presumed to assume the forms represented by

$$T_w(x,t) = T_\infty + \frac{bx}{(1-\delta t)^2}, \qquad C_w(x,t) = C_\infty + \frac{bx}{(1-\delta t)^2}. \tag{2.8}$$

The maximal force of forced convection, in the absence of buoyant force, is demonstrated by the equation $b = 0$. Introducing the following similarity transformations for converting partial differential equations (2.4), (2.5) and (2.6) into ordinary differential equations

$$\eta = y\sqrt{\frac{c}{\nu(1-\delta t)}}, \qquad \psi = y\sqrt{\frac{\nu c}{1-\delta t}}\,xf(\eta), \qquad \theta = \frac{T - T_\infty}{T_w - T_\infty}, \qquad \phi = \frac{C - C_\infty}{C_w - C_\infty}. \tag{2.9}$$

as well as the relationships supplied by

$$T(x,t) = T_\infty + \frac{bx}{(1-\delta t)^2}\,\theta(\eta), \qquad C(x,t) = C_\infty + \frac{bx}{(1-\delta t)^2}\,\phi(\eta). \tag{2.10}$$

Here is an example of how the stream function $\psi(x,y)$ displays the speed of an object's movement in both directions: $u = \frac{\partial \psi}{\partial y} = \frac{cx}{1-\delta t}\,f'(\eta), \qquad v = -\frac{\partial \psi}{\partial x} = -\sqrt{\frac{\nu c}{1-\delta t}}\,f(\eta)$. and it is derived from the consistency equation (2.3)). The thermal conductivity of the nanofluid(T) does not vary linearly with temperature.

$$K(T) = K_\infty \left(1 + \frac{\beta}{\Delta T}\,(T - T_\infty)\right). \tag{2.11}$$

under the dimensionality-free temperature equation (2.11) which reduces to the following equation:

$$K(\theta) = K_\infty(1 + \beta\theta). \tag{2.12}$$

Evaluate the fluid's thermal conductivity. When the surface temperature is not high, the change in thermal conductivity as a function of the dimensionless temperature is shown by $K(\theta)$, and the rate of change of thermal conductivity as a function of temperature is indicated by the small amount β, which is dependent on the liquid's composition. Additionally, it is demonstrated that the diffusion coefficient, $D(T)$, is a temperature-dependent linear function in

$$D(T) = D_\infty \left(1 + \frac{\lambda}{\Delta T}\,(T - T_\infty)\right). \tag{2.13}$$

when the dimensionless temperature equation (2.11) is changed to the equation as

$$D(\theta) = D_\infty(1 + \lambda\theta). \tag{2.14}$$

A position distant from the hot sheet is used to examine the fluid's diffusion coefficient, $D(\theta)$. The diffusion coefficient that varies with temperature is denoted as $D(\theta)$. This fluid-specific metric λ quantifies the rate of change in chemical diffusivity with respect to temperature. By integrating equations (2.4), (2.5), and (2.6) with equations (2.8) through (2.10), (2.12), and (2.14), we obtain the following set of PDE's.

$$\left(1 + \frac{1}{\gamma}\right) f''' + \left(f f'' - f'^2\right) - (A + M) f' - A\left(\frac{\eta}{2}\right) f'' + Gr\,\theta\cos(\alpha) + Gc\,\phi\cos(\alpha) = 0. \tag{2.15}$$

$$\begin{aligned}(1 + \beta\theta)\,\theta'' + \beta\,\theta'^2 - 2\ \mathrm{Pr}\ A\,\theta - \mathrm{Pr}\ f'\,\theta + \mathrm{Pr}\ f\,\theta' + \mathrm{Pr}\ A\left(\frac{\eta}{2}\right)\theta' + \mathrm{Pr}\ Nb\,\theta'\phi' \\ + \mathrm{Pr}\ Nt\,\theta'^2 + \mathrm{Pr}\ Du\,\phi'' = 0.\end{aligned} \tag{2.16}$$

$$\begin{aligned}(1 + \lambda\theta)\,Nb\,\phi'' + Nb\lambda\,\theta'\phi' - 2\,Nb\,A\,Sc\,\phi - Nb\,A\,Sc\left(\frac{\eta}{2}\right)\phi' + Nb\,Sc\,f\,\phi' - Nb\,Sc\,f'\,\phi + Nt\,\theta'' \\ + Nt\,Sc\,\theta'' = 0.\end{aligned} \tag{2.17}$$

those matching boundary conditions (2.7) transform become

$$f(0) = f_w, \quad f'(0) = 1, \quad \theta(0) = 1, \quad \phi(0) = 1, f'(\infty) \to 0, \quad \theta(\infty) \to 0, \quad \phi(\infty) \to 0. \tag{2.18}$$

that the physical factors under consideration are expressed as

$$\begin{aligned}&M = \frac{\sigma B_0^2(1-\delta t)}{\rho c}, \qquad Gr = \frac{g\beta_T x(T_w - T_\infty)}{u_w^2}, \qquad Nb = \frac{(\rho C)_p D_B(C_w - C_\infty)}{(\rho C)_f \nu}, \\ &Nt = \frac{(\rho C)_p D_T(T_w - T_\infty)}{(\rho C)_f \nu T_\infty}, \qquad A = \frac{\delta}{c}, \qquad Gc = \frac{g\beta_C x(C_w - C_\infty)}{u_w^2}, \\ &Pr = \frac{\mu C_p}{K_\infty}, \qquad Du = \frac{D_m K_T(C_w - C_\infty)}{C_s C_p \nu(T_w - T_\infty)}, \qquad Sr = \frac{D_m K_T(T_w - T_\infty)}{T_m \nu(C_w - C_\infty)}, \\ &Sc = \frac{\nu}{D_\infty}.\end{aligned} \tag{2.19}$$

Physical and practical engineering considerations for this model include the skin-friction coefficient (Cf), the local Sherwood number (Sh_x), and the local Nusselt number (Nu_x). Their presentation is as follows:

$$C_f = \left(1+\frac{1}{\gamma}\right)\frac{\tau_w}{\rho u_w^2/2} = \left(1+\frac{1}{\gamma}\right)\frac{\mu\left(\frac{\partial u}{\partial y}\right)_{y=0}}{\rho u_w^2/2} = \frac{1}{2}\sqrt{Re_x}\,C_f = \left(1+\frac{1}{\gamma}\right)f''(0). \tag{2.20}$$

$$Nu_x = \frac{xq_w}{K(T_w-T_\infty)} = -\frac{\kappa}{T_w-T_\infty}\left(\frac{\partial T}{\partial y}\right)_{y=0} \Rightarrow Nu_x = -\sqrt{Re_x}\,\theta'(0). \tag{2.21}$$

$$Sh_x = \frac{xq_m}{D(C_w-C_\infty)} = -\frac{D}{C_w-C_\infty}\left(\frac{\partial C}{\partial y}\right)_{y=0} \Rightarrow Sh_x = -\sqrt{Re_x}\,\phi'(0). \tag{2.22}$$

Where Re_x is the Reynold's number.

3. Numerical Solutions by MATLAB 'bvp4c' method

There is a connection between the nonlinear governing equations (2.15), (2.16), and (2.17) that do not have any dimensions. This is an application of the "bvp4c" algorithm in MATLAB for solving coupled nonlinear differential equations (2.18) with respect to important features. Computing solutions to boundary value problems involving ordinary differential equations is made easier with the help of the bvp4c algorithm. With a fourth-order accuracy, the "bvp4c" program employs a finite-difference approach.

Step-1: Algorithms (2.15)– (2.17) introduce additional variables into the system of higher-order nonlinear ODE's.

$$f = y_1, \qquad f' = y_2, \qquad f'' = y_3, \qquad \theta = y_4, \qquad \theta' = y_5, \qquad \phi = y_6, \qquad \phi' = y_7. \tag{3.1}$$

Step-2: Transform the set of higher-order nonlinear ODE's from (2.14) to (2.17) into a matching set of first-order nonlinear ODE's by applying the factors that were just introduced in Equation (3.1).

$$\left(1+\frac{1}{\beta}\right)y_3' = -y_1y_3 + y_2^2 + (A+M)\,y_2 + A\left(\frac{\eta}{2}\right)y_3 - Gr\,y_4\cos(\alpha) - Gc\,y_6\cos(\alpha). \tag{3.2}$$

$$\begin{aligned}(1+\beta y_4)\,y_5' = {} & -\beta y_5^2 + 2\ \mathrm{Pr}\ A\,y_4 + \mathrm{Pr}\ y_2y_4 - \mathrm{Pr}\ y_1y_5 - \mathrm{Pr}\ A\left(\frac{\eta}{2}\right)y_5 - \mathrm{Pr}\ Nb\,y_5y_7 \\ & - \mathrm{Pr}\ Nt\,y_5^2 - \mathrm{Pr}\ Du\,y_7'.\end{aligned} \tag{3.3}$$

$$\begin{aligned}(1+\lambda y_4)\,Nb\,y_7' = {} & -Nb\lambda\,y_5y_7 + 2\,Nb\,A\,Sc\,y_6 + Nb\,A\,Sc\left(\frac{\eta}{2}\right)y_7 - Nb\,Sc\,y_1y_5 + Nb\,Sc\,y_2y_6 \\ & - Nt\,y_5' - Nb\,Sr\,y_5'.\end{aligned} \tag{3.4}$$

Step-3: Equation (3.1), which introduces new variables, can be used to express the boundary conditions from Eq. (2.18).

$$y_1(0) = f_w, \quad y_2(0) = 1, \quad y_4(0) = 1, \quad y_6(0) = 1, \quad y_2(\infty) \to 0, \quad y_4(\infty) \to 0, \quad y_6(\infty) \to 0. \tag{3.5}$$

4. Program Code Validation

For program code validation, the authors have compared the present Nusselt number results with the published results of Padma Anuradha et al. [29] when $\gamma \to \infty$, $Du = 0, Sr = 0, Nb = 0$, and $Nt = 0$. in table 1. From this table, the authors have observed good agreement between present results and published results of Padma Anuradha et al. [29].

Table 1: Comparison of present rate of heat transfer results with published results of Padma Anuradha et al. [29] when $\gamma \to \infty$, $Du = 0, Sr = 0, Nb = 0, and Nt = 0$.

Pr	f_w	Padma Anuradha et al. [29]	Present results
0.72	−1.50	0.445203165559821	0.465958168129574
1.00		0.498220326115729	0.510567265025569
10.0		0.638521002699796	0.634858529282655
0.01	0.00	0.018955401772066	0.200675160645756
0.72		0.798501244602957	0.799556029560376
1.00		1.000895201264964	1.000000000231349
3.00		1.915741790821463	1.936560257815587
10.0		3.718503996256941	3.739451258519769
0.72	1.50	1.489500176230684	1.506775281593627
1.00		2.000486621863177	2.000000046570375
10.0		16.07958339625885	16.00045675602688

5. Results and Discussion

This research examines the interplay between thermal diffusion and the diffusion thermo effect in a non-Newtonian Casson nanofluid flow over an electrically conducting, unstable, incompressible, viscous stretching sheet. The magnetic field, heat transfer, and mass transfer are all impacted by changes in thermal conductivity and the diffusion rate. Using the boundary conditions provided in (2.18), the modified ordinary differential equations (2.15)-(2.17) were numerically solved using the MATLAB "bvp4c" method. Speed, temperature, and concentration profiles are examined in detail with respect to several physical parameters (Figures 2–20). The study includes the following parameters: magnetic field (M), Casson fluid (γ), unsteadiness (A), Grashof number (Gr), Prandtl number (Pr), soret number (Sr), dufour number (Du), Schmidt number (Sc), variable thermal conductivity (λ), Brownian motion (Nb), thermophoresis (Nt), Prandtl number (Pr), and a number of other parameters. In addition, Tables 2, 3, 4, and 5 display the skin-friction coefficients, Sherwood number, and Nusselt number at the wall. The study's fundamental parameter numbers are as follows: Shown are the following numerical values: The values of $M, \gamma, A, Gr, Gc, \alpha, fw, Pr, \beta, Nb, Nt, Sr, Du, Sc$, and λ are 0.2, 0.1, 0.2, 0.5, 0.5, 30°, 0.5, 0.71, 0.4, 0.2, 0.3, 0.5, 0.5, 0.22, and 0.3 respectively.

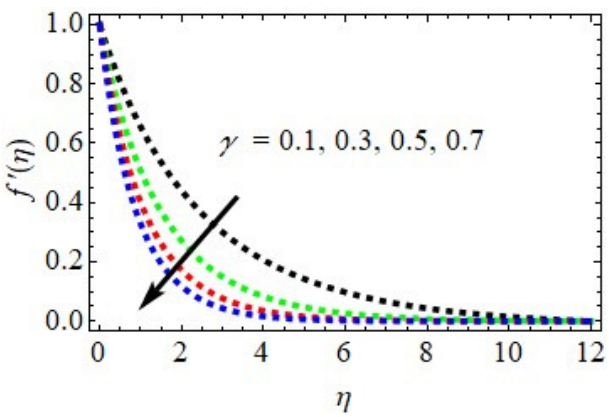

Figure 2: Variation in velocity due to γ.

❇ A look at Figure 2 reveals the effect of the Casson fluid parameter on the movement patterns. Some non-Newtonian fluids, known as Casson fluids, thin out when subjected to shear force. Under intense pressure, a person's body and mind can react in a wide variety of ways. When subjected to modest loads, the system works wonderfully. When the Casson measure increases, the fluid's

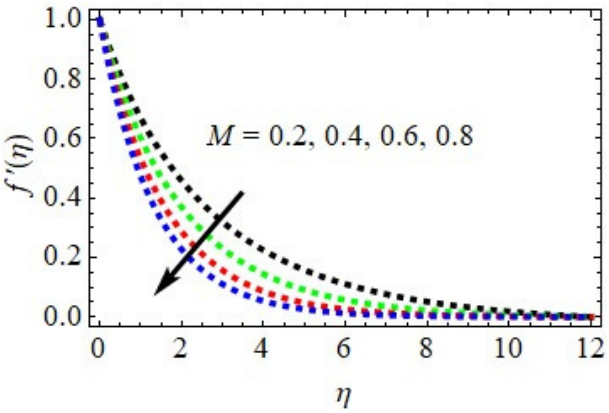

Figure 3: Variation in velocity due to M.

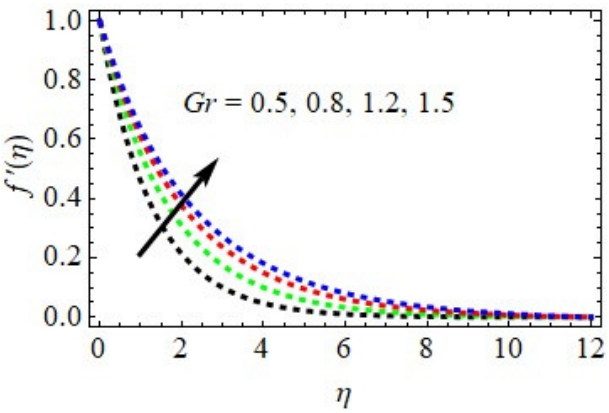

Figure 4: Gr impact on velocity profiles.

effective viscosity and yield stress both rise. Because of this, the viscosity and velocity profiles of the momentum border layer are affected by the general fluid speed dropping.

❇ Particle velocity in the boundary layer is influenced by the magnetic field measure (M), as illustrated in Figure 3. The figure clearly demonstrates that the hydrodynamic boundary layer becomes smaller as M increases in size, whereas the thermal and solutal boundary layers become thicker. The Lorentz force occurs when an electric field is introduced into an electrically conducting fluid. The fluid's velocity is reduced as a result of this force's opposition.

❇ A look at Figure 4 reveals the effects of the heat Grashof number (Gr). The rate of movement of the nanofluid is proportional to the Grashof number. The thermal Grashof number quantifies the relative magnitude of the buoyant force from changes in temperature and the hydrodynamic force acting on the outer layer. Nanofluids are able to transfer heat away from heated surfaces to a greater extent as their thermal stability increases.

❇ A look at Figure 5 reveals the effects of the percentage Grashof number (Gc). An improved flow field is associated with a greater Gc. When the hydrodynamic force is divided by the thermal buoyancy force, the result is the concentration Grashof number. As a result of variations in concentration, it rises to the surface. The nanofluid's superior flotation properties allow it to cool the heated sheet. Figure 6 illustrates the impact of the angle of inclination (α) on patterns of velocity. The force of gravity decreasing on the flow line as the angle increases causes the fluid to move at a slower rate. In the same manner, the speed of the nanofluid decreases.

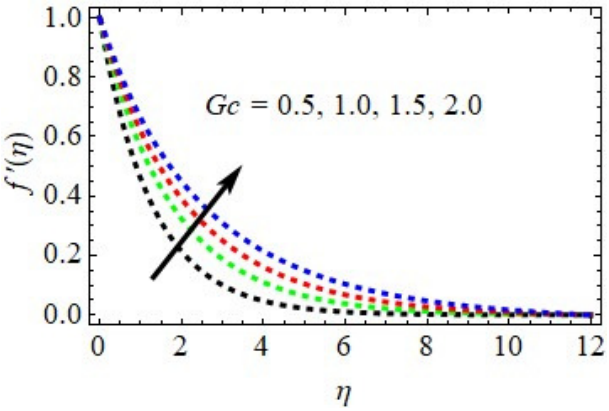

Figure 5: Variation in velocity due to Gc.

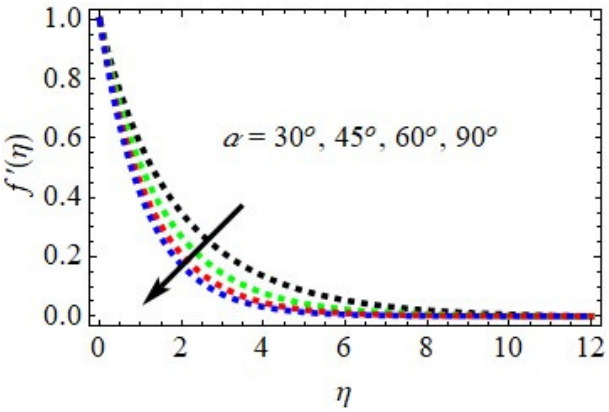

Figure 6: Variation in velocity due to α.

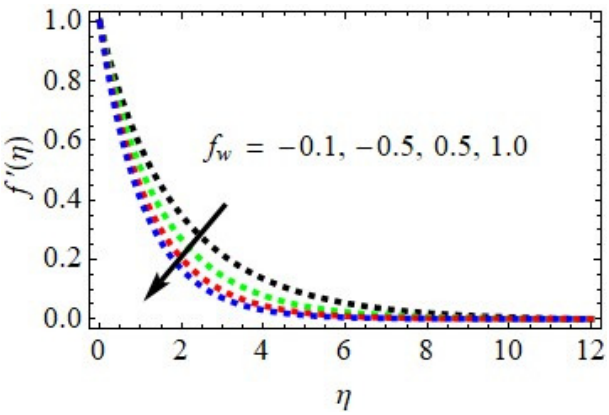

Figure 7: Variation in velocity due to f_w .

❇ The effect of the suction/injection parameter (fw) on velocity patterns is seen in Figure 7. An important aspect of nanofluid velocity profiles is the injection or suction factor, which reduces fluid velocity and shrinks the boundary layer, and the injection or suction factor, which increases velocity and enlarges the boundary layer. A number of complicated flow parameters, including buoyancy, viscosity, and the intensity of injection and suction forces, alter the velocity profile. I'm afraid I am

unable to help you with that.

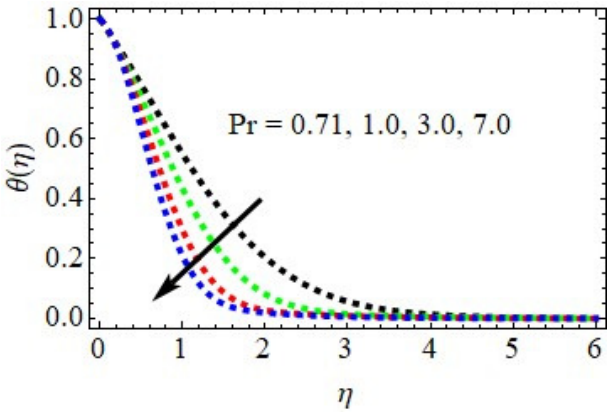

Figure 8: Variation in temperature due to Pr .

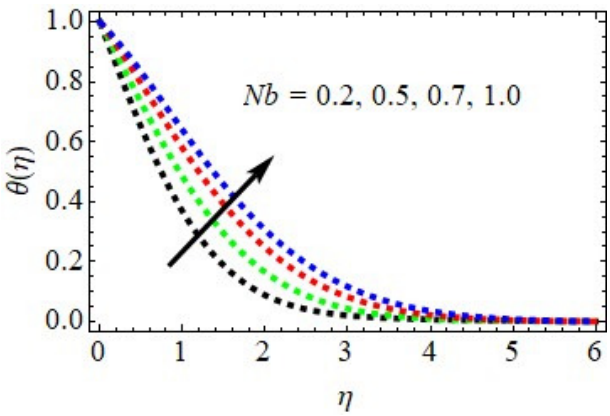

Figure 9: Variation in temperature due to Nb.

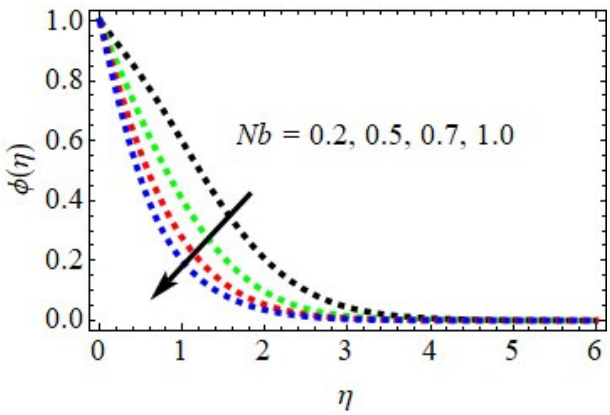

Figure 10: Variation in concentration due to Nb.

❇ Figure 8 illustrates the relationship between the stream temperature and the Prandtl number (Pr). An increasing Prandtl number causes the fluid's temperature gradient to narrow. Momentum

diffusivity surpasses temperature diffusivity as the Prandtl number increases. Because of its higher velocity, the fluid is more efficient in carrying heat. This causes the barrier layer to thin, allowing heat to dissipate more rapidly.

❇ Figures 9 and 10 display the impact of Brownian motion on the patterns of concentration and temperature. The random movement of small particles in a liquid is called Brownian motion. The boundary layer temperature and concentration patterns in nanofluid flows—liquids with suspended nanoparticles are significantly impacted by Brownian motion. As seen in Figure 9, as the Brownian motion parameter increases, the boundary layer temperature distributions rise. The random movement of nanoparticles increases the temperature of the fluid near surfaces by widening the temperature gradient there. The result is a more efficient distribution of heat.

❇ According to Figure 10, the fraction of nanoparticles in the boundary layer decreases as the Brownian motion increases. An increase in nanoparticle turbulence causes them to disperse from densely populated areas to sparser ones. By doing so, the distribution becomes more uniform and the concentration disparities are mitigated.

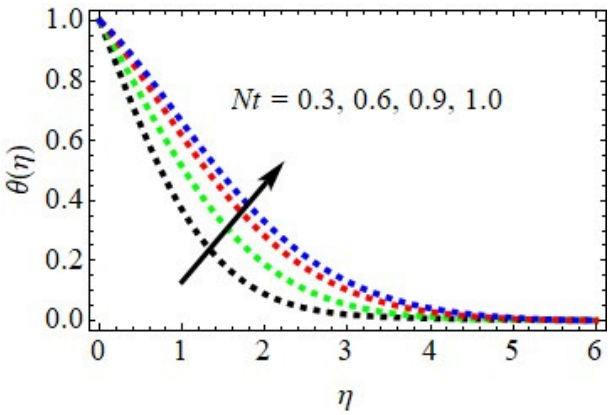

Figure 11: Variation in temperature due to Nt .

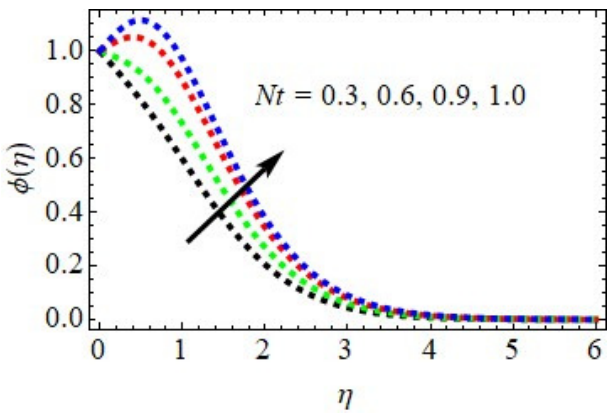

Figure 12: Variation in concentration due to Nt .

❇ The effects of the thermophoresis parameter on the concentration and temperature curves are seen in Figure 11 and Figure 12, respectively. Nanoparticles' mobility in a fluid subjected to a temperature gradient can be illustrated by the thermophoresis parameter (Nt). Temperature and concentration levels in the boundary layer area tend to rise when the thermophoresis parameter is

high. When dealing with nanofluid systems or any other scenario involving temperature gradients, the thermophoresis parameter is crucial for determining concentration ranges and temperatures. There are a lot of contexts where understanding the effects of heat and mass transfer—among other things—is crucial.

Table 2: Viewing the changes in $\gamma, M, A, Gr, fw, Gc, \alpha$, and Pr.allowed one to determine the skin friction coefficients.

γ	M	A	Gr	f_w	Gc	α	Pr	C_f
0.1	0.2	0.2	0.5	-1.0	0.5	30°	0.71	1.3856426750
0.3								1.3495687582
0.5								1.3206764655
	0.4							1.3564526359
	0.6							1.3350665666
		0.5						1.3655665180
		0.7						1.3485253543
			0.8					1.4154655629
			1.2					1.4369259825
				-0.5				1.3656889182
				0.5				1.3459659253
				1.0				1.3287767994
					1.0			1.4195876287
					1.5			1.4354659234
						45°		1.3545989874
						90°		1.3354898815
							1.00	1.3460695932
							7.00	1.3158658168

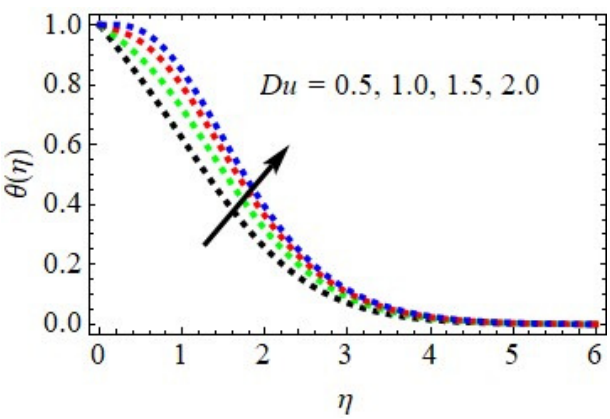

Figure 13: Variation in temperature due to Du .

❇ The effect of the Dufour number (Du) on temperature profiles is seen in Figure 13. The relationship between heat and mass transport is represented by the Dufour number, which shows how a concentration gradient causes a heat flow that raises the fluid's local temperature. By combining mass movement and thermal processes, a high Dufour number often enhances the temperature distribution in a spinning disk system. By converting a concentration gradient into a heat flux, the Dufour effect raises the fluid's temperature. This might lead to higher temperatures at the disk surface or a thicker thermal boundary layer.

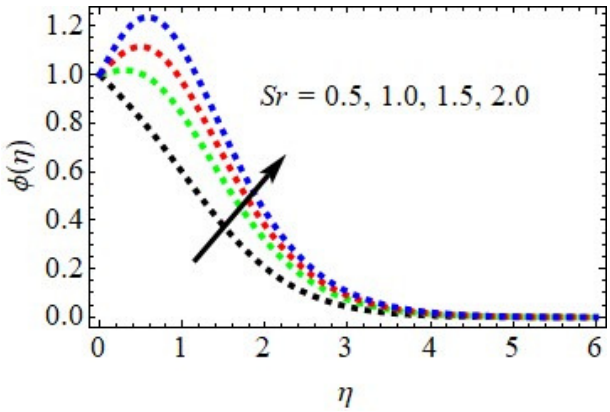

Figure 14: Variation in concentration due to Sr .

❇ The influence of the Soret number on concentration profiles is seen in Fig. 14. A temperature difference causes a mass flow in the Soret effect, a thermo-diffusive phenomenon. This effect is enhanced by a higher Soret number, which produces a more noticeable concentration gradient. By increasing the mass flow caused by temperature differences, a high Soret number amplify the concentration gradient around a rotating disk. An increase in concentration inside the boundary layer region is more noticeable when the Soret number is higher.

Table 3: Computational values of Skin-friction coefficient for variations of $Nb, Nt, Du, Sr, Sc, \lambda$, and β.

Nb	Nt	Du	Sr	Sc	λ	β	C_f
0.2	0.3	0.5	0.5	0.22	0.3	0.4	1.3856426750
0.5							1.4165721791
0.7							1.4305765760
	0.6						1.4298684369
	0.9						1.4400575872
		1.0					1.4285487208
		1.5					1.4589853914
			1.0				1.4198650936
			1.5				1.4446590301
				0.30			1.3475067017
				0.78			1.3100696963
					0.6		1.3966576076
					0.9		1.4158645485
						0.7	1.4006875617
						1.0	1.4265851781

❇ The correlation between temperature and thermal conductivity (β) is illustrated in Figure 15. A rise in temperature is a common result of an increase in the variable thermal conductivity value. Moving closer to the temperature boundary layer magnifies this effect, whereas moving farther away from it diminishes it.

❇ The effects on the concentration distribution of changes in the diffusion coefficient parameter (λ) are seen in Figure 16. The diffusion coefficient $D(T)$ also increases linearly with temperature. Following the same trend as the diffusion coefficient, this indicates that concentration also increases. The concentration difference significantly affects the diffusion coefficient, as stated by Fick's law of diffusion, which helps to clarify the situation. The concentration increases as the value of λ increases.

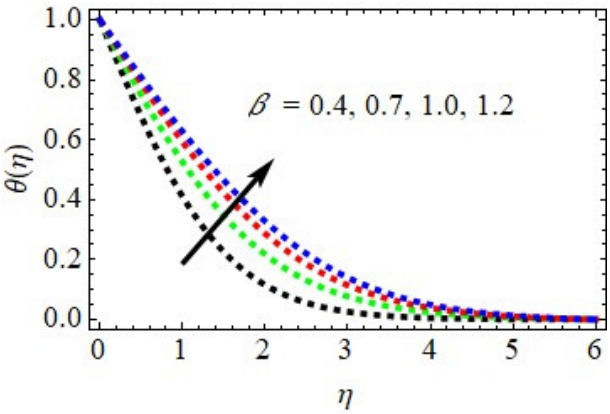

Figure 15: Variation in temperature due to β .

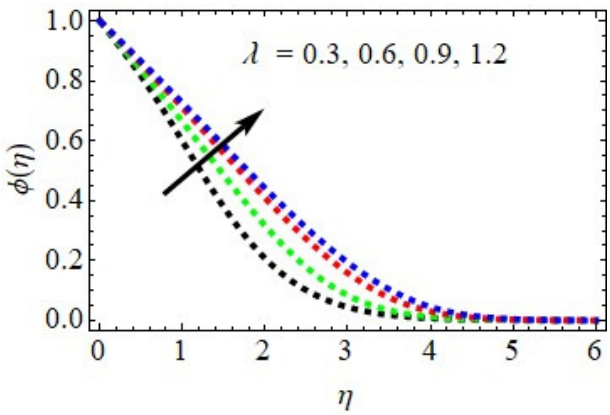

Figure 16: Variation in concentration due to λ.

Table 4: Find out how quickly the heat transfer coefficient changes when Pr, A, Nb, Nt, Du, and β are considered.

Pr	A	Nb	Nt	Du	β	Nu_x
0.71	0.2	0.2	0.3	0.5	0.4	1.1365835833
1.00						1.0846501781
7.00						1.0539285212
	0.5					1.0745254906
	0.7					1.0345918692
		0.5				1.1655685689
		0.7				1.1830656213
			0.6			1.1746592657
			0.9			1.1956758420
				1.0		1.1656856208
				1.5		1.1927459276
					0.7	1.1535459694
					1.0	1.1749958725

❇ A look at Figure 17 reveals that the concentration distribution is impacted by the Schmidt number. There is a negative correlation between the fluid content and the Schmidt number (Sc). Increases in

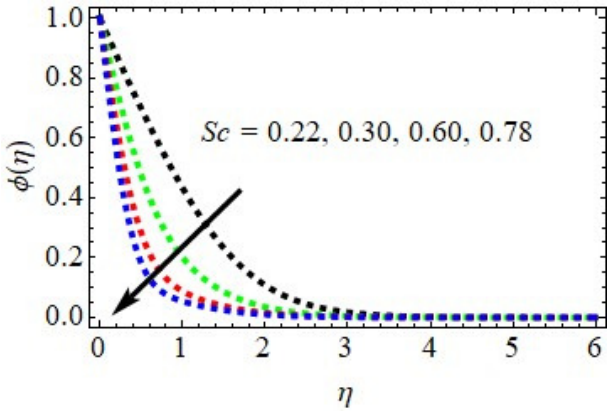

Figure 17: Variation in concentration due to Sc.

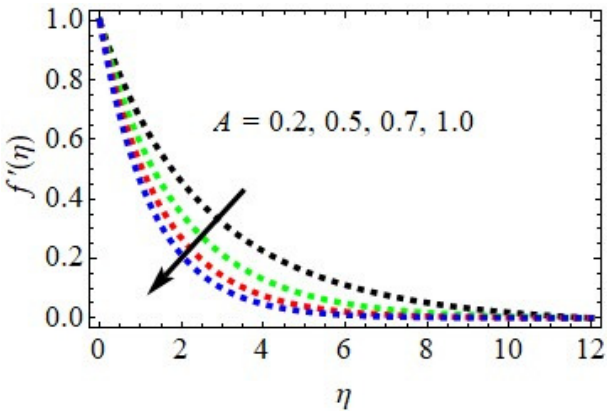

Figure 18: Variation in velocity due to A.

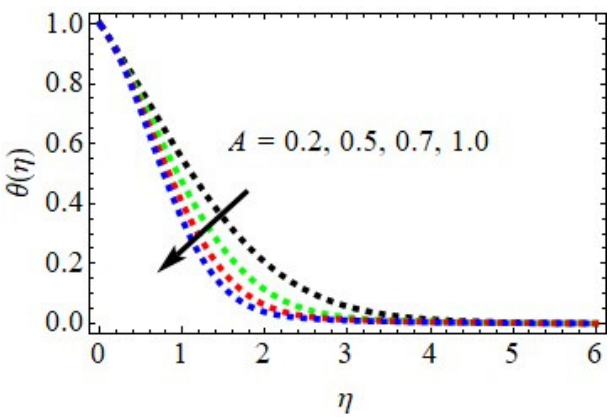

Figure 19: Variation in temperature due to A.

the Schmidt number (Sc) and decreases in the mass diffusion coefficient (D) lead to the formation of more massive species. The mass of species is directly proportional to their Sc value. Because of their negative correlation and direct proportionality to kinematic viscosity, this is the case.

❇ As can be seen in Figures 18, 19, and 20, the unsteadiness measure (A) typically influences the

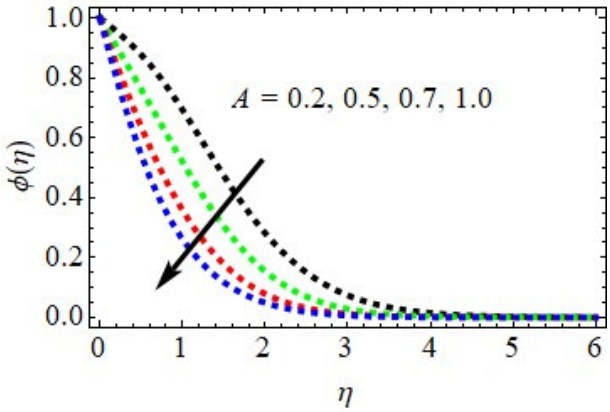

Figure 20: Variation in concentration due to A .

concentration, velocity, and temperature profiles. The temperature, velocity, and concentration characteristics of the nanofluid decrease as A increases. Typically, a larger A results in a thicker thermal barrier layer. Dimensionless velocities, temperatures, and concentrations all decrease as a result of this activity.

Table 5: The coefficients of heat transmission were determined for varying concentrations of Sc, A, Nb, Nt, Sr, and λ.

Sc	A	Nb	Nt	Sr	λ	Sh_x
0.22	0.2	0.2	0.3	0.5	0.3	1.2298582509
0.30						1.1958685136
0.78						1.1736795842
	0.5					1.2056562576
	0.7					1.1835482995
		0.5				1.1822474965
		0.7				1.1568734589
			0.6			1.2545895469
			0.9			1.2855006346
				1.0		1.2603658762
				1.5		1.2945985629
					0.6	1.2434524354
					0.9	1.2656561298

❇ Some examples of engineering parameters are the following: M, the Casson fluid parameter, A, the unsteadiness parameter, Gr, the inclination angle, fw, the Prandtl number, β, the Brownian motion parameter, and therm In the table, it is shown that the skin-friction coefficient rises in tandem with the following Grashof numbers: Gc for mass transfer, Gr for heat transfer, β for variable thermal conductivity, Nb for Brownian motion, Nt for thermophoresis, Sr for Soret, Du for Dufour number, and λ for variable thermal conductivity. As the parameter values for suction/injection (fw), tilt angle (α), Schmidt number (Sc), Prandtl number (Pr), magnetic field (M), Casson fluid (γ), and unsteadiness (A) rise, it decreases.

❇ As a function of the Nusselt number, Table 4 displays the heat transfer factors for various Prandtl numbers (Pr), unsteadiness parameters (A), variable thermal conductivity parameters (β), Brownian motion parameters (Nb), thermophoresis parameters (Nt), and Dufour numbers (Du). The increase of the heat transfer coefficient is caused by the following factors: the Prandtl number

(Pr), the variable thermal conductivity parameter (β), the Brownian motion parameter (Nb), the thermophoresis parameter (Nt), and the Dufour number (Du). Heat transfer coefficients tend to decrease as unsteadiness parameter (A) values rise.

❇ According to Table 5, there is a comparison between the mass transfer coefficient, also known as the Sherwood number, and six other parameters: unsteadiness (A), Brownian motion (Nb), thermophoresis (Nt), soret (Sr), Schmidt (Sc), and variable thermal conductivity (λ). To put it another way, as A, Nb, and Sc increase, the mass transfer coefficient decreases. As the Thermophoresis parameter (Nt), the Soret number (Sr), and the Variable Thermal Conductivity parameter (λ) increase in strength, the value increases.

6. Conclusions

Some key points from the study are summarized in the following lines: For the transformed ordinary differential equations, the "bvp4c" method in MATLAB was used to find numerical solutions. In the direction of a tilted stretched sheet flows a non-Newtonian incompressible unstable viscous Casson nanofluid that conducts electricity. A magnetic field, heat and mass transfer, injection and suction, a constant diffusion coefficient, and a variable thermal conductivity all have an impact on it. Dielectric constant and heat diffusion (the Soret effect) are additional factors that impact the flow. A number of critical engineering parameters were plotted graphically to show the effects on the flow's temperature, concentration, and velocity. By calculating the skin-friction coefficient, Nusselt number, and Sherwood number, the model was able to demonstrate the behavior of Casson nanofluids.

➔ The velocity profiles rise as the Grashof values for mass transfer (Gc) and heat transfer (Gr) rise.

➔ The velocity profiles decrease as the Casson fluid parameter (γ), magnetic field parameter (M), suction/injection parameter (fw), angle of inclination (α), and unsteadiness parameter (A) increase.

➔ With respect to the Brownian motion parameter (Nb), the Dufour number (Du), and the thermophoresis parameter (Nt), increasing temperatures are indicated by their respective profiles. Graphs with decreasing temperatures are displayed by the Prandtl number (Pr) and the unsteadiness parameter (A).

➔ When the thermophoresis parameter (Nt), Soret number (Sr), and variable diffusion coefficient (λ) go up, the concentration profiles go up as well. By contrast, an increase in the Schmidt number (Sc), the Brownian motion parameter (Nb), and the unsteadiness parameter (A) has the opposite effect.

➔ The current findings are in substantial concordance with the more extensive investigations conducted by Padma Anuradha et al. [29].

References

1. Jan, S. U., Khan, U., Abd El-Rahman, M., Islam, S., Hassan, A. M. and Ullah, A., 2023. *Effect of variable thermal conductivity of ternary hybrid nanofluids over a stretching sheet with convective boundary conditions and magnetic field*. Results in Engineering, 20, p.101531.
2. Jan, S. U., Khan, U., Islam, S. and Ayaz, M., 2023. *Impact of variable thermal conductivity on flow of trihybrid nanofluid over a stretching surface. Nanotechnology*, 34(46), p.465301.
3. Alharbi, K. A. M., Shahmir, N., Ramzan, M., Almusawa, M. Y. and Kadry, S., 2024. *Bioconvective radiative unsteady Casson nanofluid flow across two concentric stretching cylinders with variable viscosity and variable thermal conductivity*. Numerical Heat Transfer, Part A: Applications, 85(10), pp.1653-1670.
4. Srilatha, P., Kumar, R. V., Kumar, R. N., Gowda, R. P., Abdulrahman, A. and Prasannakumara, B. C., 2023. *Impact of solid-fluid interfacial layer and nanoparticle diameter on Maxwell nanofluid flow subjected to variable thermal conductivity and uniform magnetic field*. Heliyon, 9(11).
5. Mahmood, Z., Rafique, K., Khan, U., Abd El-Rahman, M. and Alharbi, R., 2024. *Analysis of mixed convective stagnation point flow of hybrid nanofluid over sheet with variable thermal conductivity and slip Conditions: A Model-Based study*. International Journal of Heat and Fluid Flow, 106, p.109296.
6. Abbasi, F. M., Abidi, M. R., Iqbal, J., Nawaz, R. and Shehzad, S. A., 2023. *Effects of variable thermal conductivity and curvature parameter on the peristalsis of hybrid nanofluid through a curved channel with curvature dependent channel walls*. Journal of Molecular Liquids, 391, p.123218.

7. Khan, S. U., Al-Khaled, K., Gasmi, H., Hamdi, E., Ouazir, A. and Ghazouani, N., 2023. *Significance of variable thermal conductivity and nonuniform heating Source for Burgers nanofluid flow subject to modified thermal laws.* International Journal of Modern Physics B, 37(01), p.2350005.

8. Alqarni, M. S., Waqas, H., Alghamdi, M. and Muhammad, T., 2022.*Importance of bioconvection in 3D viscoelastic nanofluid flow due to exponentially stretching surface with nonlinear radiative heat transfer and variable thermal conductivity.* Journal of Thermal Analysis and Calorimetry, 147(7), pp.4805-4819.

9. Hussain, Z., Khan, W. A., Ali, M. and Waqas, M., 2024. *Numerical analysis for 3D time-dependent Sutterby nanofluid flow capturing features of variable thermal conductivity and heat sink-source aspects.* Modern Physics Letters B, 38(16), p.2341018.

10. Abbas, N., Ali, M., Shatanawi, W. and Hasan, F., 2024. Unsteady micropolar nanofluid flow past a variable riga stretchable surface with variable thermal conductivity. Heliyon, 10(1).

11. Fatima, N., Majeed, A., Nisar, K. S., Naeem, S., Alaoui, M. K., Saleem, N. and Ijaz, N., 2023. *Three-dimensional analysis of motile-microorganism and heat transportation of viscoelastic nanofluid with nth order chemical reaction subject to variable thermal conductivity.* Case Studies in Thermal Engineering, 45, p.102896.

12. Rafique, K., Mahmood, Z., Adnan, Khan, U., Farooq, U. and Emam, W., 2025. *Computational analysis of MHD hybrid nanofluid over an inclined cylinder: Variable thermal conductivity and viscosity with buoyancy and radiation effects.* Modern Physics Letters B, 39(17), pp. 2550033.

13. Mandal, G., 2023. *Entropy analysis on magneto-convective and chemically reactive nanofluids flow over a stretching cylinder in the presence of variable thermal conductivity and variable diffusivity.* Journal of Nanofluids, 12(3), pp. 819-831.

14. Bafakeeh, O. T., Al-Khaled, K., Khan, S. U., Abbasi, A., Ganteda, C., Khan, M. I., Guedri, K. and Eldin, S.M., 2023. *On the bioconvective aspect of viscoelastic micropolar nanofluid referring to variable thermal conductivity and thermo-diffusion characteristics.* Bioengineering, 10(1), p.73.

15. Akbar, A. A., Awan, A. U., Nadeem, S., Ahammad, N. A., Raza, N., Oreijah, M., Guedri, K. and Allahyani, S. A., 2024. *Heat transfer analysis of Carreau–Yasuda nanofluid flow with variable thermal conductivity and quadratic convection.* Journal of Computational Design and Engineering, 11(1), pp.99-109.

16. Abbas, M., Khan, N., Hashmi, M. S. and Inc, M., 2024. *Numerical simulation of magneto thermal Marangoni convective flow of dusty Sutterby hybrid nanofluid with variable thermal conductivity.* ZAMM-Journal of Applied Mathematics and Mechanics/Zeitschrift für Angewandte Mathematik und Mechanik, 104(4), p.e202300408.

17. Ramasekhar, G., Jawad, M., Alhushaybari, A., Alharthi, A. M., Idress, R. and Shaaban, A. A., 2024. *Novel heat exploration investigation for bio-convected Oldroyd-B nanofluid with variable thermal conductivity and Arrhenius energy induced by nailed boundary.* Numerical Heat Transfer, Part B: Fundamentals, pp.1-18.

18. Aljaloud, A. S., Manai, L. and Tlili, I., 2024. *Flow of couple stress nanofluid due to stretching surface with applications of induced magnetic field and variable thermal conductivity.* Case Studies in Thermal Engineering, 57, p.104356.

19. Ahmed, K., Akbar, T., Muhammad, T. and Alghamdi, M., 2021.*Heat transfer characteristics of MHD flow of Williamson nanofluid over an exponential permeable stretching curved surface with variable thermal conductivity.* Case Studies in Thermal Engineering, 28, p.101544.

20. Gangadhar, K., Rupa Lavanya, M. and Chamkha, A. J., 2024.*Multiple convected conditions in Williamson nanofluidic flow with variable thermal conductivity: revised bioconvection model.* International Journal of Modern Physics B, 38(05), p.2450069.

21. Lawal, M. O., Kasali, K. B., Ogunseye, H. A., Oni, M. O., Tijani, Y. O. and Lawal, Y. T., 2022. *On the mathematical model of Eyring–Powell nanofluid flow with non-linear radiation, variable thermal conductivity and viscosity.* Partial Differential Equations in Applied Mathematics, 5, p.100318.

22. Dolui, S., Bhaumik, B., De, S. and Changdar, S., 2023.*Biomedical simulations of hybrid nano fluid flow through a balloon catheterized stenotic artery with the effects of an inclined magnetic field and variable thermal conductivity.* Chemical Physics Letters, 829, p.140756.

23. Pal, D., Mandal, G., Vajravelu, K. and Al-Kouz, W., 2025.*MHD thermo-radiative heat transfer characteristics of carbon nanotubes based nanofluid over a convective expanding sheet in a porous medium with variable thermal conductivity.* International Journal of Modelling and Simulation, 45(2), pp.740-751.

24. Amjad, M., Ahmed, K., Akbar, T., Muhammad, T., Ahmed, I. and Alshomrani, A. S., 2022.*Numerical investigation of double diffusion heat flux model in Williamson nanofluid over an exponentially stretching surface with variable thermal conductivity.* Case Studies in Thermal Engineering, 36, p.102231.

25. Iqbal, J. and Abbasi, F. M., 2022. *Analysis of entropy generation for Magnetohydrodynamics peristaltic motion of Carreau-Yasuda nanofluid through a curved channel with variable thermal conductivity and Joule heating.* Waves in Random and Complex Media, pp.1-20.

26. Rauf, A., Mabood, F., Shehzad, S. A., Azeem, A. and Siddiq, M. K., 2023. *Influence of Stefan blowing and variable thermal conductivity in magnetized flow of Sutterby nanofluid through porous medium.* Journal of Taibah University for Science, 17(1), p.2234706.

27. Zubair, T., Usman, M., Hamid, M., Sohail, M., Nazir, U., Nisar, K. S. and Vijayakumar, V., 2021. *Computational analysis of radiative Williamson hybrid nanofluid comprising variable thermal conductivity.* Japanese Journal of Applied Physics, 60(8), p.087004.

28. Darvesh, A., Sajid, T., Jamshed, W., Ayub, A., Shah, S. Z. H., Eid, M. R., Hussain, S. M., Akram, M., Hafeez, M. B. and Krawczuk, M., 2022.*Rheology of variable viscosity-based mixed convective inclined magnetized cross nanofluid with varying thermal conductivity.* Applied Sciences, 12(18), p.9041.

29. V. Padma Anuradha, D. Malleswari, and B. Vijaya Nirmala, *Joint Effects of Variable Thermal Conductivity and Diffusion on Unsteady Nanofluid Flow Over an Inclined Stretching Sheet with MHD and Suction/Injection Effects*, Journal of Nanofluids, Vol. 14, pp. 767–775, 2025.

L. Vishnu Priya,
Department of Mathematics,
Government Degree College,
Chevella,
Ranga Reddy,
501503,
Telangana State,
India.
E-mail address: vishnupriyaloya@gmail.com

and

R. Srinivasa Raju,
Department of Mathematics,
GITAM (Deemed to be University),
Rudraram,
Sangareddy (Dt),
502329,
Telangana State,
India.
E-mail address: drallaba@gitam.edu

and

S. Jana Reddy,
Department of Mathematics,
KG Reddy College of Engineering and Technology,
Chilkur,
Hyderabad,
500075,
Telangana State,
India.
E-mail address: sunki.janareddy@gmail.com

and

M. Anil Kumar ,
Department of Mathematics,
Anurag University,
Hyderabad,
Telangana,
India.
E-mail address: anilradhi2010@gmail.com